Quantum Field Theory of Inelastic Diffraction. I. Low-Order Perturbation Theory*

C. B. Duke and G. E. Laramore†
Department of Physics, Materials Research Laboratory and Coordinated Science Laboratory, University of Illinois, Urbana, Illinois 61801
(Received 7 December 1970)

Following the definition of the model Hamiltonian, a quantum field theory of inelastic electron scattering from a single-crystal solid is formulated. The interaction of the incident electron with the ion cores is described by the rigid-ion model. The electron-plasmon interaction is described using the random-phase-approximation analysis for jellium. The excitation of both surface and bulk modes is considered explicitly. The electron propagators are renormalized via the electron-electron interactions. Attention is focused on relating diffraction phenomena in the elastic electron-lattice scattering to the differential inelastic cross section. The "surface" conservation laws of energy and momentum parallel to the surface are a consequence of our model of the solid. The vestige of momentum conservation normal to the surface causes a new diffraction phenomenon, "sideband diffraction," in the case of the excitation of a bulk-loss mode. This phenomenon should be observable experimentally in the inelastic angular profiles associated with the excitation of bulk plasmons. The general features of both one-step and two-step inelastic diffraction are described in the simplest (kinematical) approximation. The qualitative features associated with the model predictions for the two-step process are in agreement with experimental measurements of differential inelastic cross sections.

I. INTRODUCTION

It has been recognized since the discovery[1] of low-energy electron diffraction (LEED) that diffraction phenomena in elastic-scattering channels exert a major influence on the inelastic cross sections for discrete energy losses in the range $1 \lesssim w \lesssim 30$ eV. Although this result presumably is valid for all loss energies w, at high values of $w \gtrsim 30$ eV, multiple low-energy losses obscure the observation of discrete losses. In the case of low values of $w \lesssim 1$ eV, the energy resolution ΔE of most existing spectrometers does not permit the measurement of discrete losses, i.e., $\Delta E \sim 0.5$ eV. Experimental studies of inelastic scattering in the discrete-loss regime have led to the identification of a two-step mechanism as the relevant scattering process[1-6] and to a heuristic analysis of this process.[5]

Although only two model calculations have been given for the two-step process as such[7,8] a substantial body of theoretical literature has been assembled on the general topic of inelastic particle-solid scattering. The vast majority of this literature deals with the analysis of particle-solid scattering using the Born approximation (i.e., linear-response theory) and plane-wave initial and final eigenstates for the scattered particle.[9-11] The application of this method to describe inelastic electron-solid scattering has been made for phonon excitation,[12-16] magnon excitation,[17,18] bulk-plasmon excitation,[19] and surface-plasmon excitation.[20] The simplest extension of this analysis which permits a description of the influence of elastic diffraction on the inelastic cross sections is the distorted-wave Born approximation[21] (DWBA) in which eigenstates of the (static) crystal potential rather than plane waves are used for the initial and final states of the scattered particle. This method has been used extensively in analyses of the anomolous penetration of x rays,[22] neutrons,[23] and high-energy electrons[19] in solids. Formal applications have been given to phonon-emission[24] and surface-plasmon-emission[20] inelastic processes, but the actual calculations in both cases were confined to the Born approximation in the absence of the (periodic) lattice potential. The only detailed calculation which could be classified as "using" the DWBA method is one by McRae and Jennings[25] of the cross section for a hypothetical zero-energy loss process in an ideal monatomic cubic crystal.

The next level of description above the DWBA is a quantum field theory of electron-solid scattering in which renormalization processes and the coupling of elastic and inelastic channels is included. The use of this type of theory is required by the overwhelming importance of the *inelastic* processes on determining the *elastic*-scattering cross sections in most of the energy range of LEED.[26-29] Although several formal analyses of this type have been presented,[30-32] only two actual calculations based on such a method have been performed.[7,8] In this paper we describe the theory underlying these calculations. Our analysis also augments the (formal) theoretical literature by virtue of being the first systematic quantum field theory of inelastic electron diffraction in which (i) the electron-electron-interaction-induced renormalization of both the electron propagators and the elastic electron-lattice-interaction vertices is considered explicitly,

and (ii) the surface conservation laws (energy and momentum parallel to the surface) are incorporated as an integral part of both the elastic- and inelastic-interaction vertices. In addition, we estimate the various vertex and renormalization diagrams, retain those which are relevant for discrete losses $1 \lesssim w \lesssim 30$ eV by medium-energy electrons $50 \lesssim E \lesssim 500$ eV, and calculate cross sections for both surface- and bulk-plasmon emission. The electron-diffraction conditions are shown to lead to the prediction of a new phenomenon,[7] sideband diffraction, in the inelastic cross sections associated with the excitation of bulk modes of the solid. The cross sections associated with the excitation of surface modes are shown to be dominated by the effects of instrumental resolution and the damping of the surface modes.

In retrospect, it is evident that the major manifestations in the inelastic-scattering cross sections of diffraction phenomena in the elastic-scattering cross sections are the occurrence of complementary energy-tuned and momentum-tuned (sideband-diffraction) resonances. The energy-tuned resonances are characteristic of two-step processes. For example, if a resonance occurs at an incident-beam energy E_B in the elastic cross section, it is expected to occur in the inelastic cross section at incident-beam energy E_B if diffraction occurs before loss[1] and at energy $E_B + w$ if a loss w occurs prior to diffraction.[2,3] These energy-tuned resonances are described extensively in the literature on experimental studies of inelastic diffraction.[1-6] The momentum-tuned sideband-diffraction resonances are general consequences of the vestiges of quasimomentum conservation in scattering from periodic but strongly dissipative media. They occur when the component of momentum perpendicular to the surface is "conserved" (modulo a reciprocal-lattice vector for motion normal to the surface) independent of the Bragg resonance condition at the elastic vertex. Therefore, one of their primary manifestations is maxima in the inelastic cross sections for fixed primary-beam energy E and loss energy w for directions of the scattered beam relatively far removed for the specular direction. In a kinematical model these maxima may be identified by the dependence of their location on E and w.[7,8,33]

In this paper, we construct a simple model of *inelastic* diffraction via the excitation of boson electronic loss modes simultaneously with the elastic diffraction from a rigid lattice. The model Hamiltonian is described in Sec. II. In Sec. III we specify our diagrammatic perturbation theory for the cross sections, outline the various renormalization procedures, and estimate the vertex corrections neglected in our renormalizations. Low-energy loss processes for which $w \lesssim \Delta E$ affect the *elastic* (rather than the inelastic) cross sections. An analysis of this topic has been presented elsewhere.[34] Finally, in Sec. IV we evaluate the cross sections in the simple (i.e., kinematical) limits of one- and two-step inelastic diffraction. The paper concludes in Sec. V with a summary and review of the observable consequences of the kinematical approximations to the complete theory. The results of detailed numerical calculations are presented in Paper II.

II. MODEL HAMILTONIAN

In this paper we are considering only inelastic electron-solid scattering for energy losses w in the discrete-loss range $1 \lesssim w \lesssim 30$ eV. A complete analysis of this scattering requires simultaneous consideration of the influence of electron-lattice, electron-phonon, and electron-electron interactions.[27] Such analyses have reached an advanced stage in describing the low-temperature properties of bulk metals[35] by virtue of their treatment of electron-electron interactions via expansions about the Fermi energy.[35,36] A complete analysis of LEED is complicated greatly by the failure of such expansion methods.[27] This failure causes large modifications in both the electron propagators and the electron-lattice vertices beyond those introduced by the many-body-theory extensions[35] of the one-electron models of the low-temperature properties of solids. For example, we demonstrate in Sec. III C that for electrons with large angles of incidence, plasmon-exchange vertex corrections to the independent-particle-model electron-lattice interaction can be substantial for precisely the same reasons that the plasmon-emission electron lifetimes are short[27] for electron excitation energies ϵ near and above the plasmon emission threshold[37] $\epsilon = \hbar\omega_p$.

Confronted with such difficulties in achieving an internally consistent yet tractable renormalized field theory, we decided it wisest to begin by constructing an extension to inelastic scattering of the phenomenological inelastic-collision model of elastic scattering[27,38] and using this model to investigate the major features of inelastic diffraction. Therefore, we shall consider a model in which an incident electron interacts linearly both with a rigid lattice and with a continuous boson field which describes the "discrete" electronic-loss modes (e.g., plasmons). The effects of the incoherent inelastic collisions of the incident electrons with the individual valence electrons in the solid are simulated by propagator renormalization via an energy-independent electron inelastic-collision mean free path[38] (which is equivalent to the use of a spatially uniform energy-dependent optical potential[27]). The Hamiltonian is given by

$$\mathcal{H} = \mathcal{H}_{RL} + U_{el} + \mathcal{H}_l + V_{ee} , \tag{2.1a}$$

$$\mathcal{H}_{RL} = \sum_{\vec{k}} \left(\frac{\hbar^2 k^2}{2m}\right) c^\dagger_{\vec{k}} c_{\vec{k}} + \sum_{\vec{k},\vec{q},n} c^\dagger_{\vec{k}+\vec{q}} c_{\vec{k}} B(n;\vec{k}+\vec{q},\vec{k}), \tag{2.1b}$$

$$B(n;\vec{k}+\vec{q},\vec{k}) = e^{-i\vec{q}\cdot\vec{R}_n} t_n(\vec{q},\vec{k}) , \tag{2.1c}$$

$$U_{el} = \sum_{\vec{q},\vec{k},n} c^\dagger_{\vec{k}+\vec{q}} c_{\vec{k}} T(n;\vec{k}+\vec{q},\vec{k}) , \tag{2.1d}$$

$$T(n;\vec{k}+\vec{q},\vec{k}) = e^{-i\vec{q}\cdot\vec{R}_n} h(n;\vec{k}+\vec{q},\vec{k}), \tag{2.1e}$$

$$h(n;\vec{k}',\vec{k}) = \sum_{\vec{p}} e^{-i\vec{p}\cdot\vec{R}_n} t_n(\vec{k}',\vec{k},\vec{p})(b^\dagger_{\vec{p}} + b_{-\vec{p}}), \tag{2.1f}$$

$$\mathcal{H}_l = \sum_{\vec{p}} \hbar\omega(\vec{p})(b^\dagger_{\vec{p}} b_{\vec{p}} + \tfrac{1}{2}) , \tag{2.1g}$$

$$V_{ee} = \sum_{\vec{k},\vec{k}',\vec{q}} \frac{2\pi e^2}{q^2} c^\dagger_{\vec{k}'-\vec{q}} c^\dagger_{\vec{k}+\vec{q}} c_{\vec{k}'} c_{\vec{k}} . \tag{2.1h}$$

In Eqs. (2.1), $\mathcal{H}_{RL}$ designates the rigid-lattice Hamiltonian, U_{el} the electron-loss-mode interaction, $\mathcal{H}_l$ the loss-mode Hamiltonian, and V_{ee} the residual incoherent electron-electron interactions. The $c_{\vec{k}}$ are the electron-annihilation operators; the $b_{\vec{p}}$ are those of the boson loss modes; the $t_n(\vec{k},\vec{q})$ are the individual elastic site-scattering amplitudes for the ion cores at sites located at $\vec{R}_n$ in the solid; the $t_n(\vec{k}',\vec{k},\vec{p})$ are the electron-loss-mode interaction vertices in the unit cell located at $\vec{R}_n$, and the $\hbar\omega(\vec{p})$ are the energies of these loss modes as a function of their quasimomenta $\vec{p}$. Polarization indices for these modes have been suppressed. In the case of the low-order perturbation-theory calculations presented in this paper, the only renormalizations embodied in Eqs. (2.1) are the use of site-scattering amplitudes $t_n(\vec{q},\vec{k})$ obtained from a screened pseudopotential[39–41] in the usual way.[34] If renormalizations due to lattice vibrations are included, the $t_n(\vec{q},\vec{k})$ also would depend on the temperature.[34]

The electron-electron interaction introduces proper vertex corrections in addition to screening and renormalization of the electron propagators. These corrections are important in achieving a precise theory of the low-temperature properties of metals[35] and become larger and energy dependent for energies and momenta of interest in LEED. Using our model we can estimate the plasmon-pole contributions to these vertex corrections and find that they may become large. Therefore, in any quantitative theory, an additional vertex renormalization almost certainly will be necessary.

In addition to the problems associated with many-body vertex corrections, it is not possible at the present time to give a reliable treatment of the influence of the surface on the ion-core scattering amplitudes.[29,42–44] Therefore we adopt a phenomenological point of view[27,38,44] in which the $t_n(\vec{q},\vec{k})$ are parametrized from an analysis of the elastic-scattering data and used empirically in predicting the results of inelastic-scattering experiments. For the purpose of numerical estimates in this paper, we adopt the s-wave model[38]:

$$t_n(\vec{q},\vec{k}) = t_n(E) = -h^2(e^{2i\delta_n(E)} - 1)/4\pi ikm , \tag{2.2}$$

$$\vec{k} = \vec{k}_\parallel + \vec{k}_\perp , \tag{2.3}$$

$$G^{-1}(\vec{k},E) = E - \hbar^2 k^2/2m - \Sigma(\vec{k},E) , \tag{2.4}$$

$$G^{-1}(\vec{k}(E),E) = 0 . \tag{2.5}$$

The values of the momentum parallel to the surface ($\vec{k}_\parallel$) and the total energy of the electron E are taken to be those of the incident beam.[27,38] Therefore $\vec{k}_\perp(E)$ is determined from Eq. (2.5) using $\Sigma(\vec{k},E)$ appropriate for the electron-electron interaction.[45] The s-wave phase shifts $\delta_n(E)$ are the parameters describing the electron–ion-core scattering. For purposes of obtaining numerical estimates we also use an empirical form[38] for $\Sigma(\vec{k},E)$, i.e.,

$$\Sigma(\vec{k},E) = -V - i\Gamma(E) , \tag{2.6a}$$

$$\Gamma(E) = (\hbar^2/m\lambda_{ee})[(2m/\hbar^2)(E+V)]^{1/2} , \tag{2.6b}$$

in which $\lambda_{ee} \sim 5$ Å is, by definition, twice the electron-electron-interaction-induced inelastic-collision mean free path.[38] It is approximately energy independent[38] in the region of interest ($E \gtrsim 2\hbar\omega_p$) and is the second parameter describing the elastic-scattering cross sections. The final parameter describing the elastic scattering is the inner potential V. Although it is energy dependent, estimations of it vary widely.[45–50] For simplicity, we use $V = (\zeta + \phi)$ in which ζ is the Fermi energy and ϕ is the work function of the material.

The final definitions required for the specifications of the Hamiltonian are the loss-mode dispersion relations $\omega(\vec{p})$ and their coupling vertices to the electrons $t_n(\vec{k}',\vec{k},\vec{p})$. For example, we could consider bulk and surface plasmons for which the dispersion relations are

$$\hbar\omega_b(\vec{p}) = \hbar\omega_b + \alpha p^2 , \tag{2.7}$$

and

$$\hbar\omega_s(\vec{p}) = \hbar\omega_s + \beta p_\parallel , \tag{2.8a}$$

$$p_\parallel \equiv |\vec{p}_\parallel| , \tag{2.8b}$$

respectively. However, these relations neglect plasmon damping which is important in determining the cross sections. To include this effect, it is convenient to consider the loss-mode spectral density $\Lambda_{\vec{k}_1,\ldots,\vec{k}_4}(n,m,\omega)$ defined by

$$\Lambda_{\vec{k}_1,\ldots,\vec{k}_4}(n,m,\omega) = \int_{-\infty}^{\infty} dt\, e^{i\omega t} \times \langle h^\dagger(n,\vec{k}_4,\vec{k}_3,t) h(m,\vec{k}_2,\vec{k}_1,0)\rangle_T , \tag{2.9}$$

in which $\langle\ \rangle_T$ denotes the thermal average. Inserting Eq. (2.1f) into (2.9) gives (for bulk excitations)

$$\Lambda_{\vec{k}_1,\vec{k}_2,\vec{k}_3,\vec{k}_4}(n,m,\omega) = -\sum_{\vec{p}} t_n^*(\vec{k}_4,\vec{k}_3,\vec{p})\, t_m(\vec{k}_2,\vec{k}_1,\vec{p}) \times \exp[-i\vec{p}\cdot(\vec{R}_m - \vec{R}_n)]\, N(-\omega) 2i\, \mathrm{Im} D(\vec{p},\omega)\ , \quad (2.10)$$

$$N(\omega) = [\exp(\hbar\omega/\kappa T) - 1]^{-1}\ . \quad (2.11)$$

The quantity $D(\vec{p},\omega)$ is the (retarded) propagator for the loss-mode excitation given by $(\omega \to \omega + i\delta,\ \delta \to 0^+)$,

$$D^{(0)}(\vec{p},\omega) = [\hbar\omega - \hbar\omega_0(\vec{p})]^{-1} - [\hbar\omega + \hbar\omega_0(\vec{p})]^{-1} \quad (2.12a)$$

for unrenormalized loss modes. When the interactions between the loss modes and the valence electrons are considered, the loss modes acquire a renormalization in accordance with a set of Dyson's equations.[51] In keeping with our phenomenological point of view, we shall use renormalized loss-mode propagators of the form

$$D(\vec{p},\omega) = [\hbar\omega - \hbar\omega(\vec{p}) + i\Gamma(\vec{p})]^{-1} - [\hbar\omega + \hbar\omega(\vec{p}) + i\Gamma(\vec{p})]^{-1}\ . \quad (2.12b)$$

In Eq. (2.12b) both $\omega(\vec{p})$ and $\Gamma(\vec{p})$ are to be taken from (independent) experimental measurements. Any additional multiplicative factors occurring via the theory of propagator renormalization[51] are to be absorbed in the definition of phenomenological vertex functions $t_n(\vec{k}',\vec{k},\vec{p})$.

The spectral density Λ contains in a compact form all of the information about both the electron-loss-mode interaction [via the $t_n(\vec{k}',\vec{k},\vec{p})$] and the loss-mode dispersion [via $\omega(\vec{p})$ and $\Gamma(\vec{p})$ in Eq. (2.12b)]. We have examined the influence of the general form of the coupling constants and dispersion relations on the predicted cross sections by use of two schematic models:

(i) Constant ("bulk") coupling to bulk excitations:

$$t_n(\vec{k}',\vec{k},\vec{p}) = U(\mathrm{eV\ \AA}^{9/2})\ , \quad (2.13a)$$

$$\hbar\omega(\vec{p}) = \begin{cases} \hbar\omega_{bp} + \alpha_q p^2, & \Gamma(\vec{p}) = 0 \\ \hbar\omega_{bt} + \alpha_t (p^2)^{1/2}, & \Gamma(\vec{p}) = 0 \end{cases}\ . \quad (2.13b)$$

(ii) Coherent ("semi-infinite medium") coupling to bulk excitations:

$$t_n(\vec{k}',\vec{k},\vec{p}) = p_\perp\, U'(\mathrm{eV\ \AA}^{11/2})\ . \quad (2.14)$$

More realistic calculations for aluminum[8] have been based on jellium models for the electron-plasmon coupling and the plasmon-dispersion relations. Three models have been studied in detail:

(iii) Incoherent ("bulk") coupling to bulk plasmons in jellium:

$$t_n(\vec{k}',\vec{k},\vec{p}) = [2\pi e^2(\hbar\omega_b/p^2)\,\Omega^2]^{1/2}\theta(p_c - p)\ , \quad (2.15)$$

$$\hbar\omega(\vec{p}) = \hbar\omega_b + \alpha_b p^2\ , \quad (2.16a)$$

$$\Gamma(\vec{p}) = \Gamma_0 + \beta_b p^2\ , \quad (2.16b)$$

in which Ω is the volume of a unit cell and p_c is the maximum plasmon wave number.[52]

(iv) Coherent coupling to bulk plasmons in semi-infinite jellium[31]:

$$t_n(\vec{k}',\vec{k},\vec{p}) = -i[(\pi e^2\hbar\omega_b/p^2)\,\Omega^2]^{1/2}\,\mathrm{sgn}(p_\perp)\,\theta(p_c - p)\ . \quad (2.17)$$

The plasmon-dispersion relations are given by Eqs. (2.16).

(v) Coherent coupling to surface plasmons to semi-infinite jellium:

$$t_n(\vec{k}',\vec{k},\vec{p}) = [(\pi e^2\hbar\omega_s/p_\parallel)\,\Omega^2]^{1/2}\,\delta_{p_\perp,\pm ip_\parallel}\,\theta(p_c - p_\parallel)\ , \quad (2.18)$$

$$\hbar\omega(\vec{p}_\parallel) = \hbar\omega_s + \beta_s p_\parallel\ , \quad (2.19a)$$

$$\Gamma(\vec{p}_\parallel) = \pi 2^{-4}(\hbar\omega_s)^{1/2}(\hbar^2 p_\parallel^2/2m)^{1/2}\ . \quad (2.19b)$$

In Eq. (2.18) the $\pm$ sign in the δ function is determined by the requirement that the sums in Eq. (2.1f) converge for $R_{n\perp}$ measured relative to the surface of the crystal. Note that in this case of surface excitations we insert Eq. (2.18) into Eq. (2.1f) prior to the construction of an equation analogous to Eq. (2.10)

These three jellium models and the original two schematic models complete the specification of the Hamiltonian for those cases in which we have carried out numerical calculations. The model also describes some aspects of inelastic diffraction via phonon emission.[34] We do not analyze this case in detail due to the poor energy resolution of most existing spectrometers.

III. PERTURBATION THEORY

A. Diagrammatic Prescription for the Cross Sections

A complete derivation of a diagrammatic prescription for the differential inelastic electron-solid cross sections has been given by Duke and Laramore[34] in the case of electron scattering from a vibrating lattice. The model described in Sec. II is an appropriate generalization of that case. Therefore, we restate without derivation the suitably generalized prescription in a notation appropriate for the present model.

To construct all possible terms of nth order in the interactions that contribute to the thermally averaged differential scattering cross section, we use the following rules.

(a) Draw two vertical lines, the one on the left being directed upward and the one on the right being directed downward. On these lines distribute s crosses and m dots $(s+m=n)$ with the restrictions that at least one cross or dot must be on each line and there must be an even number of dots. Label

each dot and each cross with a lattice-site index. The time variable runs upward on both lines.

(b) Completely interior line segments in this drawing (those connecting two dots and/or crosses) represent electron propagators. The four exterior line segments label the initial and final scattering states of the incident electron. Label the incoming line segments with momentum $\vec{k}_i$ and energy E_i, and the outgoing line segments with momentum $\vec{k}_f$ and energy E_f.

(c) Label each of the interior line segments by a momentum variable $\vec{k}$ and an energy variable E.

(d) Connect the dots in pairs with wavy lines representing loss-mode propagators. Label each wavy line with a frequency variable ω.

(e) Construct all topologically distinct diagrams using the preceding instructions.

(f) With each cross on the left-hand line (the upward-directed line) associate a renormalized elastic-scattering interaction vertex given by $B(n;\vec{k}_2,\vec{k}_1)$ defined by Eq. (2.1c) in which n is the ion-site label, $\vec{k}_1$ is the momentum incoming to the cross, and $\vec{k}_2$ is the momentum outgoing from the cross. With a corresponding cross on the right-hand line (the downward-directed line) associate $B^*(n;\vec{k}_2,\vec{k}_1)$. The quantity $(\vec{k}_2-\vec{k}_1)$ denotes the momentum transfer at the vertex.

(g) With a wavy line connecting two dots labeled by n and m associate a factor

$$V^2(n,m,\vec{k}_1,\vec{k}_2,\vec{k}_3,\vec{k}_4,w) = \exp[-i(\vec{k}_2-\vec{k}_1)\cdot\vec{R}_m]\exp[-i(\vec{k}_4-\vec{k}_3)\cdot\vec{R}_n] \times \Lambda_{\vec{k}_1,\vec{k}_2,\vec{k}_3,\vec{k}_4}(n,m,\omega) \quad . \tag{3.1}$$

The quantity Λ is defined by Eq. (2.10) [or its generalization given via Eqs. (2.18) and (2.19) for surface excitations] in which $w=\hbar\omega$. The dot labeled by m has an incoming electron line labeled by "1" and an outgoing line labeled by "2". If the two dots are on the same electron line the dot labeled n is associated with the incoming electron line "3" and outgoing line "4." If they are on different electron lines, the incoming line is labeled by "4" and the outgoing one by "3." Note that for the models described in Sec. II, Λ is independent of the $\{\vec{k}_1,\ldots,\vec{k}_4\}$ subscripts.

(h) With each interior line segment in the left-hand line, we associate a retarded electron propagator G_R, given by Eq. (2.4), and with each interior line segment in the right-hand line we associate an advanced electron propagator $G_A=G_R^*$. The energy and momentum of the propagator are specified by the labels on the line segment.

(i) With each dot and cross we associate energy-conserving δ functions

$$2\pi\delta(E_1-E_2-\epsilon\hbar\omega) \quad , \quad 2\pi\delta(E_1-E_2) \quad ,$$

respectively, where E_1 is the energy variable of the incoming electron propagator, E_2 is the energy variable of the outgoing electron propagator, ω is the frequency variable for a loss-mode line attached to the dot, and ϵ is $+1$ (-1) if the loss-mode line leaves (enters) the dot.

(j) Multiply the factors associated with each diagram by

$$(m^2/h^4)(|\vec{k}_f|/|\vec{k}_i|)\,\delta(E_i-E_f-\textstyle\sum_\gamma \hbar\omega_\gamma)^{-1} \quad ,$$

where the ω_γ are the frequency variables of the loss-mode propagators connecting dots on the left-hand line to those on the right-hand line. Sum over all energy and momentum labels for the electron propagators and all frequency variables labeling the loss-mode propagators. Finally, sum over all site indices labeling the dots and crosses.

In concluding this description of the diagrammatic prescription, we note that it contains vertex renormalizations associated with multiple electron scattering in a single cell [see, e.g., Eq. (60) of Ref. 34] but does not contain the subplane renormalization characteristic of the inelastic-collision model of elastic LEED [see, e.g., Eq. (73) of Ref. 34].

B. Propagator Renormalization

The lowest-order contributions to the scattering cross section arising from self-energy corrections to a propagator line are shown in Fig. 1. It is convenient to represent their contribution to the (elastic) scattering cross section as

$$\left(\frac{d^2\sigma}{dE\,d\Omega}\right)^{(3a)} = [A_{2a}\bar{B}_1+\bar{A}_{2a}B_1]\,\delta(E_f-E_i) \quad , \tag{3.2a}$$

$$B_1=\frac{2\pi m}{h^2}\sum_n t_n(E_i)\exp[-i(\vec{k}_f-\vec{k}_i)\cdot\vec{R}_n] \quad , \tag{3.2b}$$

$$A_{2a}=\frac{2\pi m}{h^2}\sum_{\vec{k}_1,n,m}\exp[-i(\vec{k}_1-\vec{k}_i)\cdot\vec{R}_m-i(\vec{k}_f-\vec{k}_1)\cdot\vec{R}_n] \times\sum_{\vec{p}}|t(\vec{p})|^2\exp[-i\vec{p}\cdot(\vec{R}_m-\vec{R}_n)]\,G[E_i-\hbar\omega(\vec{p})] \quad . \tag{3.2c}$$

In evaluating A_{2a} we noted that the vertex functions $t_n(\vec{k}',\vec{k},\vec{p})$ depend only on $\vec{p}$ for the models defined in Sec. II. Hence we designate them by $t(\vec{p})$. We also used the undamped loss-mode propagator Eq. (2.12a) for simplicity.

In the limit that we formally consider the medium to be uniform, the sums over $\vec{R}_n$ and $\vec{R}_m$ give momentum δ functions leading to

$$A_{2a}=(2\pi m/h^2)\,\delta_{\vec{k}_i,\vec{k}_f}\,\Sigma(\vec{k}_i,E_i) \quad , \tag{3.3a}$$

$$\Sigma(\vec{k}_i,E_i)=\textstyle\sum_{\vec{p}}|t(\vec{p})|^2\,G[E_i-\hbar\omega(\vec{p})] \quad . \tag{3.3b}$$

Except for a normalization factor of the unit-cell volume, in the case of bulk plasmons [model (iii)], the quantity $\Sigma(\vec{k}_i,E_i)$ is the usual plasmon-pole contribution to the electronic self-energy[52] in the limit that $(k_i-k_F)>p_c$. The quantity $k_F=(3\pi^2n)^{1/3}$

is the Fermi wave number. In deriving Eqs. (3.3) we neglected all umklapp processes resulting from the lattice sums because we regard Eqs. (2.1d)–(2.1f) as discrete representations of the electron interactions with a continuous long-wavelength boson field.

A similar result also is obtained when the lattice sums are performed directly for the finite lattice following the method of Duke, Anderson, and Tucker.[38] In the case of bulk excitations we proceed via the following sequence of operations: (a) perform the sum over the components of $\vec{R}_n$ and $\vec{R}_m$ parallel to the surface; (b) integrate over d^3k_1 using the δ function on $\vec{k}_{1\parallel}$ resulting from step (a); (c) sum over the components of $\vec{R}_n$ and $\vec{R}_m$ normal to the surface; and (d) integrate over d^3p. Portions of the last two steps are reversed for surface excitations. If we neglect umklapp terms resulting from step (a) and change the notation such that $\vec{k}_i \to \vec{k}$ and $\vec{k}_f = \vec{k}'$, then we obtain at the completion of step (b)

$$A_{2a} = \frac{2\pi m}{\hbar^2}\frac{(2\pi)^2}{A}\delta(\vec{k}'_\parallel - \vec{k}_\parallel)\left(-\frac{im}{\hbar^2 A}\right) \times \int \frac{d^3p}{(2\pi)^3}\frac{|t(\vec{p})|^2}{k_\perp[\vec{k}_\parallel - \vec{p}_\parallel,\ E - \hbar\omega(\vec{p})]} \times \sum_{n,m} \exp\{-i(\vec{k}' - \vec{p})\cdot\vec{R}_{n\perp} + i(\vec{k} - \vec{p})\cdot\vec{R}_{m\perp} + i\vec{k}_\perp[\vec{k}_\parallel - \vec{p}_\parallel,\ E - \hbar\omega(\vec{p})]|\vec{R}_{n\perp} - \vec{R}_{m\perp}|\} \quad . \tag{3.4}$$

The quantity

$$k_\perp[\vec{k}_\parallel - \vec{p}_\parallel,\ E - \hbar\omega(\vec{p})] \equiv k_\perp(E, \vec{p}_\parallel)$$

is the solution to the equation

$$E - \hbar\omega(\vec{p}) - \hbar^2(\vec{k}_\parallel - \vec{p}_\parallel)^2/2m - \Sigma[\vec{k}_\parallel - \vec{p}_\parallel, k_\perp, E - \hbar\omega(\vec{p})] = 0 \quad , \tag{3.5}$$

and A is the surface area of a unit cell. Let us consider the case of forward scattering in which $\vec{k}'\cdot\vec{R}_{n\perp}$, $\vec{k}\cdot\vec{R}_{n\perp} > 0$. If the lattice sums are performed directly we obtain

$$A_{2a} = \frac{2\pi m}{\hbar^2}\left(-\frac{im}{\hbar^2}\right)\frac{(2\pi)^2\delta(\vec{k}'_\parallel - \vec{k}_\parallel)}{1 - R(k_\perp - k'_\perp)}\int\frac{d^3p}{(2\pi)^3}\left|\frac{t(\vec{p})}{A}\right|^2\frac{1}{k_\perp(E,\vec{p})}\left(\frac{1}{1 - R[k_\perp(E,\vec{p}_\parallel) + p_\perp - k'_\perp]} + \frac{1}{1 - R[k_\perp(E,\vec{p}_\parallel) - p_\perp + k_\perp]}\right), \tag{3.6}$$

$$R(k_\perp) = e^{ik_\perp d} \quad , \tag{3.7a}$$

$$k_\perp = k_{\perp 1} + ik_{\perp 2}, \quad k_{\perp 2} > 0 \tag{3.7b}$$

in which d is the layer spacing, i.e., the depth of a unit cell. The fact that factors of $(1-R)^{-1}$ occur in Eq. (3.6) is a direct consequence of our using a lattice-periodic boson field rather than a continuous one. Another manifestation of the lattice periodic field is the factor of the unit-cell volume Ω in the $t(\vec{p})$ given by Eqs. (2.15), (2.17), and (2.18). The limit of a continuous field is achieved by taking the $d \to 0$ limit in Eq. (3.6) and using the result that $dA = \Omega$ to cancel the Ω^2 factor in $|t(\vec{p})|^2$. Thus $\tilde{t}(\vec{p}) = t(\vec{p})/\Omega$ is independent of Ω. Taking this limit, we get

$$A_{2a} \xrightarrow{\text{continuum limit}} \frac{2\pi m}{\hbar^2}\frac{im}{\hbar^2}\frac{(2\pi)^2\delta(\vec{k}'_\parallel - \vec{k}_\parallel)}{k'_\perp - k_\perp}\int\frac{d^3p}{(2\pi)^3}|\tilde{t}(\vec{p})|^2 \times\left[\frac{1}{k_\perp(E,\vec{p}_\parallel)}\left(\frac{1}{k_\perp(E,\vec{p}_\parallel) + p_\perp - k'_\perp} + \frac{1}{k_\perp(E,\vec{p}_\parallel) - p_\perp + k_\perp}\right)\right] . \tag{3.8}$$

To interpret Eq. (3.8) we first note that when we make a self-energy insertion in an intermediate state of the form shown in Fig. 2, an extra integral over d^3k' occurs. In this integral the $(2\pi)^2\delta(\vec{k}'_\parallel - \vec{k}_\parallel)$ gives forward scattering parallel to the plane of the crystal and the $(k'_\perp - k_\perp)^{-1}$ factor acts like the function $2\pi i\delta(k'_\perp - k_\perp)$ in the integral over $k'_\perp$. Thus Eq. (3.8) for the self-energy insertion does produce forward scattering. Indeed, setting $k'_\perp = k_\perp$ inside the integral over d^3p and using Eq. (3.5) to convert the quantity in braces into a factor of $G_0(\vec{k} - \vec{p}, E - \hbar\omega(\vec{p}))$ leads to

$$A_{2a} = \frac{2\pi m}{\hbar^2}\left(-\frac{i(2\pi)^2\delta(\vec{k}'_\parallel - \vec{k}_\parallel)}{k'_\perp - k_\perp}\right)\Sigma_B(\vec{k}_\parallel, k_\perp, E), \tag{3.9}$$

in which $\Sigma_B(\vec{k}_\parallel, k_\perp, E)$ is the bulk-single-boson (e.g., plasmon[52]) exchange self-energy in which $\vec{k}_\parallel$ and E are determined by the corresponding external

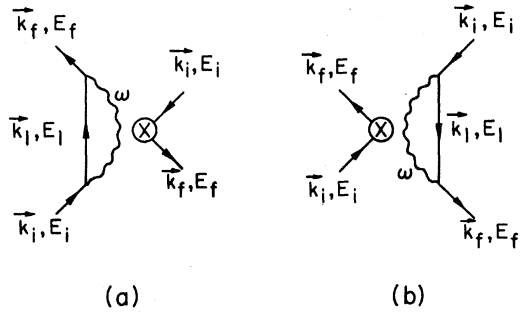

FIG. 1. Diagram for the lowest-order loss-mode self-energy contributions to the elastic-scattering cross sections. These contributions are the interference terms between the Born amplitude for rigid-lattice scattering and the amplitude for the diffuse, predominantly forward scattering of the electron from virtual inelastic excitations in a dissipative medium.

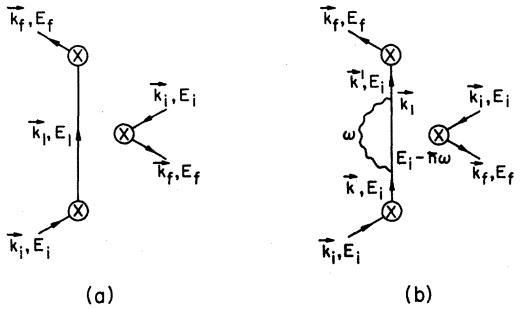

FIG. 2. Diagram for the lowest-order loss-mode self-energy insertion, (b), in the intermediate state of a contribution to the rigid-lattice cross section, (a), which is third order in the electron–ion-core scattering amplitude.

quantities and $k_\perp$ is the value projected out by the $(k'_\perp - k_\perp)^{-1}$ factor in an integral over d^3k'. Therefore Eq. (3.9) is directly comparable to the formal infinite-medium result given by Eqs. (3.3).

Propagator renormalization via the use of Fig. 3 for the electron propagator is an immediate consequence of Eq. (3.9). The $(2\pi m/\hbar^2)$ prefactor is associated with a diagram of any order via steps (i) and (j) in our prescription given in Sec. III A. The quantity in large parentheses in Eq. (3.9) removes the extra momentum integral in iterated versions of Fig. 3(b). Therefore we arrive at the inelastic-collision-model result, postulated by Duke and Tucker,[27] that in the case of bulk loss modes we can replace "bare" G_0 propagators by

$$G = G_0(1 - G_0\Sigma)^{-1} \tag{3.10}$$

The incorporation into the theory of propagator renormalization associated with surface-plasmon loss modes is more complicated because the self-energy exhibits a logarithmic divergence for forward scattering rather than one proportional to $(k'_\perp - k_\perp)^{-1}$. The systematic use of a distorted wave set of basis states seems required for a description of these renormalization processes.

In our present phenomenological model, implicitly we already are including propagator renormalizations in the propagator specificed by Eq. (2.4). Evidently the complete renormalization procedure[35,36,53] involves using the full electron-electron-interaction-induced self-energy in Eqs. (2.4) and (3.10) rather than just the plasmon-pole term given by Eq. (3.3b). As vertex renormalization also occurs, one must solve a complete coupled set of Dyson's equations for the renormalized vertices and propagators: a task beyond the scope of the present analysis. Subsequently in this paper, we consider all propagator renormalizations to be included by the use of Eqs. (2.4)–(2.6) for $G(\vec{k}, E)$.

C. Vertex Corrections

The lowest-order contributions to the (elastic) scattering cross section which exhibit the form of vertex corrections are indicated diagrammatically in Fig. 4. Their contribution to the cross section is of the form

$$\left(\frac{d^2\sigma}{dE\,d\Omega}\right)^{(4a)} = \delta(E_i - E_f)\left[(A_{3a}\overline{B}_1 + \overline{A}_{3a}B_1)\right] , \tag{3.11a}$$

$$A_{3a} = \frac{2\pi m}{\hbar^2} \sum_{\substack{1,2,3,\\ \vec{k}_1,\vec{k}_2}} \exp[-i(\vec{k}_2 - \vec{k}_1)\cdot\vec{R}_2]\, t_{n_2}$$

$$\times [E_i - \hbar\omega(\vec{p})] \sum_{\vec{p}} |t(\vec{p})|^2$$

$$\times \exp[-i(\vec{k}_f - \vec{k}_2 - \vec{p})\cdot\vec{R}_3 - i(\vec{k}_1 - \vec{k}_i + \vec{p})\cdot\vec{R}_1]$$

$$\times G(\vec{k}_1, E_i - \hbar\omega(\vec{p}))\, G(\vec{k}_2, E_i - \hbar\omega(\vec{p})) \ . \tag{3.11b}$$

We have used free-boson propagators [Eq. (2.12a)] for convenience and will take $t_{n_2}[E_i - \hbar\omega(\vec{p})]$ to be independent of n_2 {i.e., to be $t[E - \hbar\omega(\vec{p})]$}.

The evaluation of A_{3a} proceeds via the sequence of steps described above Eq. (3.4). The result just prior to the integration over $k_{1\perp}$ and $k_{2\perp}$ is (setting $\vec{k}_i \equiv \vec{k}$, $\vec{k}_f \equiv \vec{k}'$)

$$A_{3a} = \frac{2\pi m}{\hbar^2} \sum_{\vec{g}} \frac{(2\pi)^2}{A^2}\, \delta(\vec{k}'_\parallel - \vec{k}_\parallel - \vec{g}) \int \frac{d^3p}{(2\pi)^3}\, |t(p)|^2\, t[E - \hbar\omega(\vec{p})] \int \frac{dk_{1\perp}}{2\pi}\, G(\vec{k}_\parallel - \vec{p}_\parallel, k_{1\perp}, E_i - \hbar\omega(\vec{p}))$$

$$\times \int \frac{dk_{2\perp}}{2\pi}\, G(\vec{k}'_\parallel - \vec{p}_\parallel, k_{2\perp}, E - \hbar\omega(\vec{p})) \sum_{1,2,3} \exp\{-i[(\vec{k}' - \vec{k}_2 - \vec{p})\cdot\vec{R}_{3\perp} + (\vec{k}_1 - \vec{k} + \vec{p})\cdot\vec{R}_{1\perp} + (\vec{k}_2 - \vec{k}_1)\cdot\vec{R}_{2\perp}]\}\, e^{-i\vec{g}\cdot\vec{a}_2} \ , \tag{3.12}$$

in which $\vec{a}_2$ is the displacement of the central lattice site for the $\vec{R}_2$ sum from its position in the top ($\vec{R}_2 = 0$) layer. The strong maxima at forward scattering of both plasmon vertices suggests the restriction $R_{1\perp}$, $R_{3\perp} \leq R_{2\perp}$, and leads to the result that the transition from the incident to the gth scattered beam *must* occur at the lattice scattering associated with the $\vec{R}_2$ sum. This fact already is embodied in Eq. (3.12) in which $\vec{g}$ is the external beam index as described by Duke, Anderson, and Tucker.[38] A description of the procedure for carrying out the sums over the $\{\vec{R}_i\}$ when $\vec{g} \neq 0$ is given in Appendix A. Proceeding by first performing the $k_{\perp i}$ integrals and subsequently the sums over $\vec{R}_2$, $\vec{R}_1$, and $\vec{R}_3$ (in that order) gives

$$A_{3a}=\frac{2\pi m}{\hbar^2}\sum_{\vec{g}}(2\pi)^2\delta(\vec{k}_{\parallel}'-\vec{k}_{\parallel}-\vec{g})(1-\exp\{i[(k_{\perp}'+k_{\perp})d-\vec{g}\cdot\vec{a}]\})^{-1}$$
$$\times\left(-\frac{mi}{\hbar^2}\right)^2\int\frac{d^3p}{(2\pi)^3}\left|\frac{t(p)}{A}\right|^2\frac{t[E-\hbar\omega(\vec{p})]}{1-\exp\{i[(\tilde{k}_{\perp}+\tilde{k}_{\perp}')d-\vec{g}\cdot\vec{a}]\}}$$
$$\times\left(\frac{1}{1-\exp[i(k_{\perp}+\tilde{k}_{\perp}'-p_{\perp})d-i\vec{g}\cdot\vec{a}]}+\frac{1}{1-\exp[i(k_{\perp}'+\tilde{k}_{\perp}+p_{\perp})d-i\vec{g}\cdot\vec{a}]}\right), \quad (3.13a)$$

$$\tilde{k}_{\perp}\equiv k_{\perp}[\vec{k}_{\parallel}-\vec{p}_{\parallel}, E-\hbar\omega(\vec{p})], \quad (3.13b)$$

$$\tilde{k}_{\perp}'\equiv k_{\perp}[\vec{k}_{\parallel}'-\vec{p}_{\parallel}, E-\hbar\omega(\vec{p})]. \quad (3.13c)$$

In Eqs. (3.13) $k_{\perp}(\vec{k}_{\parallel}, E)$ is given by Eq. (3.5).

To estimate the quantity A_{3a} we consider the $\vec{g}=0$ case. As noted in Appendix A, the continuum nature of the loss-mode field introduces no additional simplification in Eq. (3.13) due to the backscattering nature of the elastic scattering from the lattice in the "intermediate" state (see, e.g., Fig. 4). If we neglect the E dependence of $t(E)$, we can rewrite Eq. (3.13) as

$$A_{3a}\simeq F_{3a}B_1, \quad (3.14a)$$

$$F_{3a}\equiv\int\frac{d^3p}{(2\pi)^3}\frac{|t(p)|^2}{1-\exp\{i[(\tilde{k}_{\perp}+\tilde{k}_{\perp}')d]\}}$$
$$\times\left(\frac{1}{1-\exp[i(k_{\perp}+\tilde{k}_{\perp}'-p_{\perp})d]}+\frac{1}{1-\exp[i(k_{\perp}'+\tilde{k}_{\perp}+p_{\perp})d]}\right). \quad (3.14b)$$

Noting that for parameters of interest (i.e., $E\simeq 100$ eV, nonglancing incidence),

$$k_{\perp}, k_{\perp}'\gg p_{\perp}, p_{\parallel}; \quad E\gg\hbar\omega(\vec{p}),$$

we can write

$$F_{3a}\simeq\frac{2}{\{1-\exp[i(k_{\perp}+k_{\perp}')d]\}^2}\int\frac{d^3p}{(2\pi)^3}|t(p)|^2. \quad (3.15)$$

If we further neglect the exponential factors in the strong-damping limit, we obtain

$$F_{3a}\sim 2(4\pi e^2p_c)\hbar\omega_b(mA/\hbar^2)(md^2/\hbar^2), \quad (3.16)$$

which is a quantity of order unity or larger. In addition, Eqs. (3.14) and (3.15) indicate that the vertex correction depends on the beam parameters due to the lattice-diffraction resonances. Consequently, the vertex corrections may be large and may exhibit resonances at certain values of the beam parameters.

In conclusion, it seems relevant to recall that the vertex correction calculated above is the plasmon-pole contribution to the electron-electron-interaction vertex correction. This contribution occurs *in addition to* those estimated in the low-energy case,[35,36] associated with incoherent particle-hole excitations. Authors[40,41] often allege that they use "realistic" electron-ion interactions despite their neglect of both kinds of vertex corrections. Not only can these corrections be substantial (see also Refs. 35 and 36), but we have demonstrated above that they may depend on the beam parameters E and θ for values of these parameters of interest in LEED.

IV. QUALITATIVE FEATURES OF LOW-ORDER PERTURBATION THEORY

A. Single-Step Diffraction (Born Approximation)

Single-step elastic diffraction is associated with the contribution to the cross section indicated in Fig. 5 but calculated using renormalized propagators and electron-lattice interaction vertices. Within the spirit of our phenomenological approach, we do not consider explicitly the vertex corrections and incorporate propagator renormalization via our use of Eqs. (2.4)–(2.7) together with

$$[k_{\perp 1}(\vec{g}, E)+ik_{\perp 2}(\vec{g}, E)]^2=k^2(E)-(\vec{k}_{\parallel}+\vec{g})^2 \quad (4.1)$$

to determine the internal wave vector of the electron in terms of its external beam parameters E and $\vec{k}_{\parallel}$. In terms of this model the contribution to the cross section associated with the diagram shown in Fig. 5 (the "kinematical" approximation) is

$$\left(\frac{d^2\sigma}{dE\,d\Omega}\right)^{(2)}=\delta(E'-E)|B_1|^2. \quad (4.2)$$

In Eq. (4.2) B_1 is defined by Eq. (3.2b). For identical ion-core-scattering factors, it becomes the well-known result[27]

$$B_1(\vec{k}_{\parallel}, \vec{g}, E)=\frac{2\pi mt(E)}{\hbar^2}\frac{(2\pi)^2}{A}$$
$$\times\delta(\vec{k}_{\parallel}'-\vec{k}_{\parallel}-\vec{g})[1-R(\vec{k}_{\parallel}, \vec{g}, E)]^{-1}, \quad (4.3a)$$

$$R(\vec{k}_{\parallel}, \vec{g}, E)=\exp\{i[(k_{\perp}(0, E)+k_{\perp}(\vec{g}, E))d-\vec{g}\cdot\vec{a}]\}, \quad (4.3b)$$

in which $k_{\perp}(\vec{g}, E)$ is defined via Eq. (4.1). Equations (4.3) predict broadened maxima in the intensity

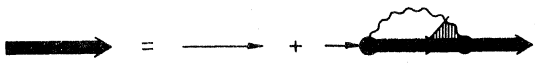

FIG. 3. Diagrammatic version of Dyson's equation for the renormalization of the electron propagator due to the electron's interaction with the loss modes alone.

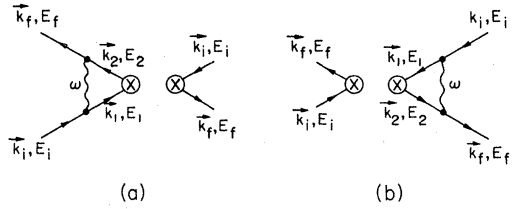

FIG. 4. Diagram for the lowest-order loss-mode vertex corrections to the Born approximation to the elastic-scattering cross section.

profiles at the "kinematical" Bragg energies determined by the solutions to

$$k_{\perp 1}(0, E) + k_{\perp 1}(\vec{g}, E) = 2\pi m/d + \vec{g}\cdot\vec{a}/d \qquad (4.4)$$

for the scattered beam labeled by $\vec{g}$. The presence of intralayer multiple scattering causes appreciable effects on these cross sections only at energies $E \lesssim 50$ eV for short inelastic-collision mean free paths ($\lambda_{ee} \sim 5$Å).[27,29,38,44]

The analogous Born-approximation expression[12-20] for the inelastic scattering is obtained from the diagram shown in Fig. 6 to be

$$\left(\frac{d^2\sigma}{dE\,d\Omega}\right)^{(2)} = \left[\frac{E-w}{E}\right]^{1/2}\left[\frac{-iN(-w)}{\pi}\right] \times \int \frac{d^3p}{(2\pi)^3}\,|A(\vec{k}', \vec{k}, \vec{p})|^2\,\mathrm{Im}D(\vec{p}, w)\,, \qquad (4.5a)$$

$$A(\vec{k}', \vec{k}, \vec{p}) = (2\pi m/\hbar^2)\textstyle\sum_n t_n(\vec{p})\exp[-i(\vec{k}' - \vec{k} - \vec{p})\cdot\vec{R}_n]\,. \qquad (4.5b)$$

Because the consequences of Eqs. (4.5) depend on the case under consideration, we consider its application to describe the emission of surface plasmons, incoherently excited bulk plasmons, and coherently excited bulk plasmons in turn.

In the case of surface plasmons, we recall that the $\vec{p}$ integrations in Eqs. (4.5) are interpreted as an integral only over $\vec{p}_\parallel$ with $p_\perp = \pm ip_\parallel$. [See Eqs. (2.18) and (2.19).] We obtain for $w \gg \kappa T$ in the continuum limit as defined in Appendix A,

$$\left(\frac{d^2\sigma}{dE\,d\Omega}\right)^{(2)}_{sp} = \left(\frac{E-w}{E}\right)^{1/2}\frac{2\pi m}{\hbar^2}\,\hbar\omega_s\,\frac{\pi m e^2 A}{\hbar^2|\vec{k}'_\parallel - \vec{k}_\parallel|} \times\left(\frac{1}{(k'_{\perp 1} - k_{\perp 1})^2 + (|\vec{k}'_\parallel - \vec{k}_\parallel| + k'_{\perp 2} + k_{\perp 2})^2}\right) \times\left(\frac{2\Gamma(|\vec{k}'_\parallel - \vec{k}_\parallel|)}{[w - \hbar\omega(|\vec{k}'_\parallel - \vec{k}_\parallel|)]^2 + \Gamma^2(|\vec{k}'_\parallel - \vec{k}_\parallel|)}\right)\,. \qquad (4.6)$$

As expected, the cross sections are largest near the forward direction ($\vec{k}'_\parallel \sim \vec{k}_\parallel$, $k'_{\perp 1} \sim k_{\perp 1}$). However, the cross section is nonzero even in the specular reflection geometry ($\vec{k}'_{\perp 1} = -\vec{k}_{\perp 1}$), because the inelastic-collision damping causes $k_\perp$ to be complex. The loss-mode lifetime-broadened energy-conservation δ function causes a conelike distribution of inelastically scattered electrons about the specular direction for energetically permitted transitions $\hbar\omega_s(0) \le w \le \hbar\omega_s(p_c)$. In particular, the maximum amplitude of the inelastic-scattering cross sections occurs for values of $\vec{k}'_\parallel$ such that

$$|\vec{k}'_\parallel - \vec{k}_\parallel| = p_\parallel(w)\,, \qquad (4.7a)$$

$$\hbar\omega_s[\,p_\parallel(w)] = w\,. \qquad (4.7b)$$

In deriving Eq. (4.7b) we presume, of course, the emission of only a single loss-mode quantum.

Equation (4.6) also predicts a maximum in the cross section for forward scattering: $k'_\perp = k_\perp$, $\vec{k}'_\parallel = \vec{k}_\parallel$. However, this equation is derived by calculating the sum over $\vec{R}_n$ in Eq. (4.5) only for $R_{n\perp} > 0$. Such a prescription is appropriate solely for bulk excitations. For plane-wave (i.e., undamped) electrons, we can add to Eq. (4.6) the contributions from the sum over $R_{n\perp} < 0$. The resulting expression for $(d^2\sigma/dE\,d\Omega)$ is obtained by multiplying Eq. (4.6) by

$$4|\vec{k}'_\parallel - \vec{k}_\parallel|^2/[(k'_{\perp 1} - k_{\perp 1})^2 + (\vec{k}'_\parallel - \vec{k}_\parallel)^2]$$

and setting $k'_{\perp 2} = k_{\perp 2} = 0$. It gives the well-known result[31] for the probability of surface-plasmon emission by high-energy electrons ($E \gtrsim 10^3$ eV). The problems inherent in adding the contributions for $R_{n\perp} < 0$ to those for $R_{n\perp} > 0$ in the case of damped excitations inside the solid (i.e., the case for which the inelastic-collision model orignally was formulated to describe[27]) are discussed further in connection with Eq. (4.16).

In the case of incoherent coupling to bulk plasmons [Eqs. (2.15) and (2.16)] we obtain from Eqs. (4.5)

$$\left(\frac{d^2\sigma}{dE\,d\Omega}\right)^{(2)}_{ibp} = \left(\frac{E-w}{E}\right)^{1/2}\frac{2\pi m\hbar\omega_b}{\hbar^2}\,\frac{2\pi m}{\hbar^2}\,\frac{e^2\Omega^2}{A}\int_0^{p_c}\frac{dp_\perp}{2\pi} \times\frac{1}{|k'_\parallel - k_\parallel|^2 + p_\perp^2}\,\frac{2\Gamma(\vec{k}'_\parallel - \vec{k}_\parallel, p_\perp)}{[w - \hbar\omega(\vec{k}'_\parallel - \vec{k}_\parallel, p_\perp)]^2 + \Gamma^2(\vec{k}'_\parallel - \vec{k}_\parallel, p_\perp)} \times\left(\left|\frac{1}{1 - R(k_\perp, k'_\perp, p_\perp)}\right|^2 + \left|\frac{1}{1 - R(k_\perp, k'_\perp, -p_\perp)}\right|^2\right)\,, \qquad (4.8a)$$

$$R(k_\perp, k'_\perp, p_\perp) \equiv \exp[i(\vec{k}_\perp - \vec{k}'_\perp + \vec{p}_\perp)\cdot\vec{d}]\,. \qquad (4.8b)$$

We have not taken the continuum limit (although umklapp processes in $\vec{k}_\parallel$ have been neglected because we expect $p_c \ll |\vec{g}|$).

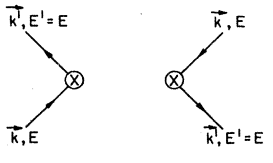

FIG. 5. Diagram for the Born approximation for the elastic-scattering cross section.

Equations (4.8) illustrate a new feature of inelastic reflection spectroscopy from a lattice-periodic loss-mode spectrum: sideband diffraction.[7] This phenomenon is predicted in the reflection geometry $\vec{k}'_{\perp 1}\cdot\vec{d}=-k'_{\perp 1}d$ because the factors of $|(1-R)|^{-2}$ in Eqs. (4.8) exhibit maxima when

$$k_{\perp 1}+k'_{\perp 1}\pm p_\perp = 2\pi s/d\ . \tag{4.9}$$

In a given experiment, the detector angle and final-state energy determine $\vec{k}'_\parallel$ and hence

$$\vec{p}_\parallel = \vec{k}'_\parallel - \vec{k}_\parallel \tag{4.10a}$$

is determined uniquely. However, energy conservation [in the $\Gamma\to 0$ limit] relates the specified loss energy w to the energy of the excitation $\hbar\omega(p)$. As $\vec{p}_\parallel$ is determined by Eq. (4.10a) the energy-conservation condition determines $p_\perp$ via

$$w=\hbar\omega[\vec{p}_\parallel, p_\perp(w,\vec{p}_\parallel)]\ . \tag{4.10b}$$

In fact, in the $\Gamma\to 0$ limit, the $p_\perp$ integral in Eq. (4.8a) is replaced by the density of states

$$\rho(\vec{p}_\parallel, w)=\left(\frac{\partial[\hbar\omega(\vec{p}_\parallel,p_\perp)]}{\partial p_\perp}\right)^{-1}_{\vec{p}_\parallel,p_\perp(\vec{p}_\parallel,w)}\ . \tag{4.11}$$

Therefore momentum conservation normal to the surface is not a selection rule determining the quantum numbers of the internal beam. Its vestiges in this case are the two sideband-diffraction resonances in the cross section for $s=0$ in Eq. (4.9). These are most easily observed by varying the angle of the detector while holding all the other beam parameters fixed.[7]

The relationship between sideband diffraction and momentum conservation is even more obvious in the continuum limit which leads to (Appendix A):

$$\left(\frac{d^2\sigma}{dE\,d\Omega}\right)^{(2)}_{\text{ibp}}=\left(\frac{E-w}{E}\right)^{1/2}\frac{2\pi m\hbar\omega_b}{h^2}\ \frac{2\pi m e^2 A}{h^2}$$
$$\times\int_0^{p_c}\frac{dp_\perp}{2\pi}\ \frac{1}{|\vec{k}'_\parallel-\vec{k}_\parallel|^2+p_\perp^2}\ \frac{2\Gamma}{[w-\hbar\omega(\vec{k}'_\parallel-\vec{k}_\parallel,p_\perp)]^2+\Gamma^2}$$
$$\times\{[(k'_{\perp 1}-k_{\perp 1}-p_\perp)^2+(k_{\perp 2}+k'_{\perp 2})^2]^{-1}$$
$$+[(k'_{\perp 1}-k_{\perp 1}+p_\perp)^2+(k_{\perp 2}+k'_{\perp 2})^2]^{-1}\}\ . \tag{4.12}$$

In the absence of the inelastic-collision damping of the electrons (i.e., $k_{\perp 2}\to 0$), the sideband-diffraction maxima at $(k'_{\perp 1}-k_{\perp 1}\pm p_\perp)=0$ become forward-scattering momentum-conservation δ functions, $\delta_{k'_\perp,\,k_\perp\pm p_\perp}$ in a fashion similar to that described in Sec. III B. However, Eq. (4.12) predicts some inelastic scattering even in the case of reflection geometry. In this case, $k'_{\perp 1}<0$ in Eq. (4.12) and $k_\perp$ and $k'_\perp$ are determined by the experimental external beam parameters $\vec{k}_\parallel, E$ and $\vec{k}'_\parallel, E'$, respectively. These contributions to the cross sections are of the same order of magnitude as the diffuse back-scattering self-energy contributions to the elastic cross sections (Sec. III B). Therefore, they usually are small near normal incidence relative to the elastic lattice-assisted back scattering. This fact renders it unlikely that the contributions to the cross sections associated with the diagrams shown in Fig. 6 can be distinguished from the diffuse background in observed reflection-geometry inelastic cross sections. Indeed, this analysis explains why two-step rather than one-step diffraction is observed in reflection-geometry experiments.[1-6]

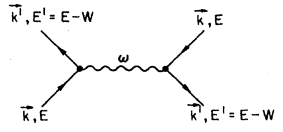

FIG. 6. Diagram for the Born approximation for the loss-mode-assisted inelastic-scattering cross section. This diagram designates the process of "single-step" inelastic diffraction.

The final topic of interest in this section is the distinction between coherent and incoherent coupling of the incident electron to the loss-mode boson field. The microscopic origin of this difference in coupling is the boundary condition at the surface satisfied by the loss-mode field.[18,31] In the case of bulk plasmons, the requirement that the electrostatic field of the plasmon vanish outside the medium is the cause of the factor $\text{sgn}(p_\perp)/2i$ in Eq. (2.17). This factor requires that the contributions to the cross section for $p_\perp>0$ add coherently to those for $p_\perp<0$ rather than incoherently as in Eqs. (4.8) and (4.12). The analog of Eq. (4.8a) in this case is given by

$$\left(\frac{d^2\sigma}{dE\,d\Omega}\right)^{(2)}_{\text{cbp}}=\left(\frac{E-w}{E}\right)^{1/2}\frac{2\pi m\hbar\omega_b}{h^2}\ \frac{\pi m e^2\Omega^2}{h^2 A}$$
$$\times\int_0^{p_c}\frac{dp_\perp}{2\pi}\ \frac{1}{|\vec{k}'_\parallel-\vec{k}_\parallel|^2+p_\perp^2}\ \frac{2\Gamma}{[w-\hbar\omega(\vec{k}'_\parallel-\vec{k}_\parallel,p_\perp)]^2+\Gamma^2}$$
$$\times\left|\,[1-R(k_\perp,k'_\perp,p_\perp)]^{-1}-[1-R(k_\perp,k'_\perp,-p_\perp)]^{-1}\right|^2\ , \tag{4.13}$$

where $R(k_\perp, k'_\perp, p_\perp)$ is given by Eq. (4.8b). The most significant distinction between Eqs. (4.13) and (4.8) occurs in the limit that $p_\perp\to 0$. In this case the quantity in large parentheses under the $p_\perp$ integral in Eq. (4.8a) becomes approximately constant whereas the analogous quantity in Eq. (4.13) vanishes linearly in $p_\perp$. This is the result that led us to define the schematic models (i) and (ii) in Sec. II. Model (i) simulates incoherent coupling and model (ii) coherent coupling. We shall find in the final (fourth) paper[54] of this series[34,54,55] that the form of the electron-loss-mode coupling exerts a substantial influence on the inelastic angular intensity profiles predicted by the model.

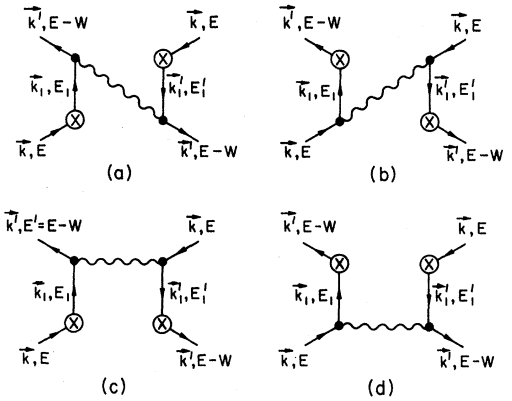

FIG. 7. Four diagrams which contribute to the inelastic cross sections associated with "two-step" inelastic diffraction: (a) the physical process of diffraction prior to loss; (b) the process of loss prior to diffraction; (c)-(d) interference processes associated with the coherent nature of the two types of contributions to inelastic diffraction.

B. Two-Step Inelastic Diffraction

Two-step inelastic diffraction is the term which has been used[1-7] to label the contributions to the inelastic differential cross section associated with electron-scattering processes in which the incident electron once scatters from the rigid lattice and once undergoes an inelastic collision involving a discrete energy loss. The fact that a scattering from the rigid lattice is involved in the processes implies that fine structure in the elastic-electron-scattering cross sections will be reflected in the inelastic cross sections. In its usual form,[1-6] this concept is kinematical in nature with both the elastic and inelastic vertices being single-scattering events. Therefore, it is the direct analog in an inelastic channels of the double-diffraction approximation in the elastic channel.[38] Although several extensions of this concept to include multiple scattering in each of the elastic and inelastic events separately can be made easily,[34,54] for clarity we confine our attention here to the double-scattering limit. It is the simplest approximation in which we achieve our objective, noted in the Introduction, of assessing the influence of *elastic* diffraction on the *inelastic* cross sections. Experimentally, the existence of a strong influence of this nature has been amply documented.[1-6]

The four diagrams describing the possible fourth-order inelastic-scattering processes which include a rigid-lattice scattering in each propagator line are illustrated in Fig. 7. After some manipulation, the sum of their contributions to the cross section may be written as

$$\left(\frac{d^2\sigma}{dE\,d\Omega}\right)^4=\left(\frac{E-w}{E}\right)^{1/2}\frac{1}{2\pi}\int\frac{d^3p}{(2\pi)^3}\left[-2iN(-w)\,\mathrm{Im}\,D(\vec{p},w)\right]$$
$$\times\left[\left|A_{2b}(\vec{k}',\vec{k},\vec{p},E)+A_{2c}(\vec{k}',\vec{k},\vec{p},E-w)\right|^2\right], \tag{4.14a}$$

$$A_{2b}(\vec{k}',\vec{k},\vec{p},E)=\int\frac{d^3k_1}{(2\pi)^3}\,A(\vec{k}',\vec{k}_1,\vec{p})$$
$$\times G(\vec{k}_1,E)T_1(\vec{k}_1,\vec{k},E)\,, \tag{4.14b}$$

$$T_1(\vec{k}',\vec{k},E)=\sum_m B(m;\vec{k}',\vec{k})$$
$$=\sum_m t_m(E)\exp[-i(\vec{k}'-\vec{k})\cdot\vec{R}_m]\,, \tag{4.14c}$$

$$A(\vec{k}',\vec{k},\vec{p})=(2\pi m/h^2)\sum_n t_n(\vec{p})$$
$$\times\exp[-i(\vec{k}'-\vec{k}-\vec{p})\cdot\vec{R}_n]\,, \tag{4.5b}$$

$$A_{2c}(\vec{k}',\vec{k},\vec{p},E-w)=\int\frac{d^3k_1}{(2\pi)^3}\,T(\vec{k}',\vec{k}_1,E-w)$$
$$\times G(\vec{k}_1,E-\omega)A(\vec{k}_1,\vec{k},\vec{p})\,. \tag{4.14d}$$

Comments in experimental papers[2-6] notwithstanding, the amplitudes for the "diffraction before loss" (A_{2b}) and "loss before diffraction" (A_{2c}) processes are added *coherently* because they connect the same initial and final states. If we take $w\gg\kappa T$ and use the free loss-mode propagator, Eq. (2.12a), then

$$-2iN(-w)\,\mathrm{Im}\,D(\vec{p},w)\Rightarrow 2\pi\delta(w-\hbar\omega(\vec{p}))\,. \tag{4.15}$$

In this limit our formalism reduces to that of the conventional quantum field theory.[56] Therefore the cross sections may be specified by the bremsstrahlung diagrams for A_{2b} and A_{2c} directly, a notation which was used by Duke, Laramore, and Metze[7] in their analysis of two-step inelastic diffraction predicted by model (i) in Sec. II.

Our next task is the specification of A_{2b} and A_{2c} in the various special cases. As usual, we consider cases in which $t_n(E)$ and $t_n(\vec{p})$ are independent of n (i.e., identical scattering layers for both the elastic and inelastic vertices). The analysis proceeds as indicated above Eq. (3.4). Our only restriction[57] on the sums over the loss-vertex sites (labeled by n) and the elastic vertex sites (labeled by m) is that because of the forward-scattering nature of the loss processes, the loss must occur closer to the surface than the elastic event, i.e., $R_{m_\perp}\geq R_{n_\perp}$. The final result for the surface-plasmon case in the $w\gg\kappa T$ limit is given by[58]

$$\left(\frac{d^2\sigma}{dE\,d\Omega}\right)^{(4)}_{sp}=\left(\frac{E-w}{E}\right)^{1/2}\frac{2\pi m\hbar\omega_s}{h^2}\,\frac{m\pi e^2\Omega^2}{h^2A}$$
$$\times\sum_{\vec{g}}\left|1-R(k_\perp(0,E),k'_\perp(0,E-w),ip_\parallel,\vec{g})\right|^{-2}$$
$$\times\left|A_b(\vec{g},E)+A_c(\vec{g},E-w)\right|^2\frac{1}{|\vec{k}'_\parallel-\vec{k}_\parallel-\vec{g}|}$$
$$\times\frac{2\Gamma(\vec{k}'_\parallel-\vec{k}_\parallel-\vec{g})}{[w-\hbar\omega(\vec{k}'_\parallel-\vec{k}_\parallel-\vec{g})]^2+\Gamma^2(\vec{k}'_\parallel-\vec{k}_\parallel-\vec{g})}\,, \tag{4.16a}$$

$$R(k_\perp', k_\perp, p_\perp, \vec{g}) = \exp[i(k_\perp + k_\perp' + p_\perp)d - i\vec{g}\cdot\vec{a}] , \quad (4.16b)$$

$$A_b(\vec{g}, E) = -\frac{mit(E)}{\hbar^2 A k_\perp(\vec{g}, E)} \frac{1}{1 - R[k_\perp(0, E), k_\perp(\vec{g}, E), \vec{g}]} , \quad (4.16c)$$

$$R(k_\perp', k_\perp, \vec{g}) = \exp[i(k_\perp' + k_\perp)d - i\vec{g}\cdot\vec{a}] , \quad (4.16d)$$

$$A_c(\vec{g}, E-w) = \frac{mit(E-w)}{\hbar^2 A k_\perp'(-\vec{g}, E-w)} \times \frac{1}{1 - R[k_\perp'(-\vec{g}, E-w), k_\perp'(0, E-w), \vec{g}]} . \quad (4.16e)$$

The $k_\perp(\vec{g}, E)$ are defined by Eq. (4.1). Comparison of the single-diffraction expression [Eq. (4.6)] with Eq. (4.1) reveals that the only difference between the two expressions is the factor of $\sum_{\vec{g}} |A_b(\vec{g}) + A_c(\vec{g})|^2$. Near maxima in A_b and A_c this extra term can become quite large, making the two-step diffraction dominate the single-step diffraction. Furthermore the single-step diffraction exhibits no structure related to similar structure in the elastic channel. However, $A_b(\vec{g})$ mirrors structure in the elastic intensity profile at the energy E_b at which it occurs. The quantity $A_c(\vec{g})$ mirrors this structure at the higher energy $E = (E_B + w)$. Therefore experimental correlation of structure at E_B in the elastic intensity profile with similar structure at *both* E_B and $E_B + w$ in the inelastic profiles[4-6] constitutes *prima facie* evidence that the two-step diffraction process dominates the single-step process. This remark is true for both bulk- and surface-loss-mode excitations. However, a distinguishing characteristic of surface plasmons, evident in both Eqs. (4.6) and (4.16), is the appearance of a local minimum in the inelastic cross sections in the specular direction because of the conelike distribution of the inelastically scattered electrons as discussed in Sec. IV A.

Essentially identical results describe two-step inelastic diffraction via the excitation of a bulk-loss mode. If $w \gg \kappa T$, the cross sections associated with the sum of the diagrams shown in Fig. 7 are given by

$$\left(\frac{d^2\sigma}{dE\,d\Omega}\right)_{bp}^{(4)} = \left(\frac{E-w}{E}\right)^{1/2} \frac{2\pi m\hbar\omega_b}{h^2} \frac{m\pi e^2\Omega^2}{h^2 A} \sum_{\vec{g}} \int_0^{p_c} \frac{dp_\perp}{2\pi} \frac{1}{(\vec{k}_\parallel' - \vec{k}_\parallel - \vec{g})^2 + p_\perp^2} \frac{2\Gamma(\vec{k}_\parallel' - \vec{k}_\parallel - \vec{g}, p_\perp)}{[w - \hbar\omega(\vec{k}_\parallel' - \vec{k}_\parallel - \vec{g}, p_\perp)]^2 + \Gamma^2} \times M[k_\perp(0, E), k_\perp'(0, E-w), p_\perp, \vec{g})] |A_b(\vec{g}, E) + A_c(\vec{g}, E-w)|^2 . \quad (4.17a)$$

The quantity $|A_b + A_c|^2$ is identical to that occurring in Eq. (4.16a) and reflects structure in the elastic-scattering cross sections. The factor $M(k_\perp, k_\perp', p_\perp, \vec{g})$ depends on the incoherent or coherent nature of the electron-plasmon vertex. It is given by

$$M_{ibp}(k_\perp, k_\perp', p_\perp, \vec{g}) = 2(|1 - R(k_\perp, k_\perp', p_\perp, \vec{g})|^{-2} + |1 - R(k_\perp, k_\perp', -p_\perp, \vec{g})|^{-2}) , \quad (4.17b)$$

$$M_{cbp}(k_\perp, k_\perp', p_\perp, \vec{g}) = |[1 - R(k_\perp, k_\perp', p_\perp, \vec{g})]^{-1} - [1 - R(k_\perp, k_\perp', -p_\perp, \vec{g})]^{-1}|^2 \quad (4.17c)$$

in the two cases, respectively. The function $R(k_\perp, k_\perp', p_\perp, \vec{g})$ is defined by Eq. (4.16b).

A set of remarks parallel to those made below Eqs. (4.16) apply to Eqs. (4.17). The one- and two-step cross sections are identical except for the extra factor of $|A_b + A_c|^2$ in the two-step case. Sideband diffraction occurs in the case of bulk-loss modes because of the $M(k_\perp, k_\perp', p_\perp, \vec{g})$ factors. For small values of $p_\perp$, M_{ibp} approaches a constant whereas $M_{cpb} \propto p_\perp$. Therefore, as in the surface-plasmon case, the single- and two-step inelastic-diffraction angular intensity profiles (fixed incident beam parameters, varying final angles, fixed loss energy) are similar in structure. However, their energy intensity profiles (fixed angles, varying incident beam energy, fixed loss energy) are quite different because of the modulating factor $|A_b + A_c|^2$ in the two-step expressions.

V. SUMMARY AND CONCLUSIONS

In Sec. II of this paper we constructed a model description of the interaction of an electron incident on a solid with both the (rigid) lattice potential and various loss modes characteristic of the solid. In Sec. III we specified a diagrammatic method for calculating the electron-solid scattering cross sections. This method was applied to demonstrate that propagator renormalization associated with bulk-loss modes leads simply and directly to the inelastic-collision model of Duke and Tucker.[27] Vertex corrections due to loss-mode exchange processes were estimated. They seem to be substantial for back-scattered electrons and, in addition, depend sensitively on both the incident beam energy and angle. From this result we infer that their neglect in any quantitative theory is a serious omission. However, in our phenomenological model we formally can incorporate them into empirically determined renormalized vertex functions.

Presuming that we could construct suitably renormalized vertices and propagators, we evaluated in Sec. IV both the single- and two-step inelastic-

scattering cross sections for a discrete energy loss $1 \lesssim w \lesssim 30$ eV. Our major conclusion is that although they both exhibit comparable orders of magnitude, only the two-step process is modulated as a function of incident beam energy E in resonance with similar modulations of the elastic intensity profiles. In particular, this resonance occurs both at the energy E and at $E+w$. As such a relation between the modulations of the elastic and inelastic cross sections is observed experimentally,[1-6] it is evident that in such cases two-step inelastic diffraction dominates single-step inelastic diffraction near maxima in the cross sections (i.e., the Born approximation is manifestly inadequate to describe inelastic electron-solid scattering).

The appropriate conservation laws to describe both elastic- and inelastic-scattering processes are those of energy and the component of momentum parallel to the planar face of the single-crystal solid. The vestiges of conservation of momentum normal to the surface lead only to sideband-diffraction resonances in the angular intensity profiles, for the excitation of bulk loss modes.[7] These conservation laws are built into our model, and its predictions seem to be in accord with experimental data.

In Sec. IV we derived and discussed several features of the predicted cross sections which could lead to the experimental distinction between bulk and surface loss modes and between various types of electron-bulk-loss-mode coupling. As these features depend on the values of the model parameters, their discussion is deferred until the following paper[54] in which we evaluate the two-step inelastic-electron-scattering cross sections from W(100) and Al(100) using the various models constructed in Sec. II. Our current work is devoted to as precise as possible a test of the model in the (most-favorable) case of aluminum. If the model provides an adequate interpretation of experimental data in this test case, we intend to apply it to describe scattering from other materials (most notably Ag and W) for which the identification of the various mechanisms for inelastic electron diffraction is uncertain.

ACKNOWLEDGMENTS

The authors are indebted to Professor F. M. Propst, Professor M. B. Webb, and Dr. J. O. Porteus for discussions of the experimental situation and unpublished copies of their data.

APPENDIX

In the text of this paper we have several occasions to perform multiple sums over lattice positions normal to the surface. In general, these sums contain lattice-site indices associated with both electron–ion-core interactions and electron-loss-mode interactions. As written in Sec. II, the electron-loss-mode interactions exhibit the periodicity of the lattice. In this case, we use a convenient device to perform nested sums over a loss-mode index ν_1 and an ion-core index ν_2. Note that if $\vec{a}$ is the shift in the position of the central cell from one layer to the next, then for most simple crystal faces [e.g., all low-index faces of cubic crystals but not the (0001) face of hexagonal crystals], $(n+1)\,\vec{a}=\vec{R}_{\parallel}$, where n is the number of layers between identical layers and $\vec{R}_{\parallel}$ is a lattice vector parallel to the surface. Thus, for example, a typical double sum over layers for the (100) face of an fcc or bcc lattice takes the form

$$S_1 = d\sum_{\nu_1=0}^{\infty} \exp[ik'_{\perp} d\nu_1] \sum_{\nu_2=\nu_1}^{\infty} \exp[ik_{\perp} d\nu_2 - i\vec{g}\cdot\vec{a}_2] \times \exp[ik|\nu_2-\nu_1|], \qquad \text{(A1)}$$

in which $\vec{a}_2$ is the shift in the location of the central unit cell for the layer indexed by ν_2. In the case of the (100) face, we can write $\vec{a}_2=\nu_2\vec{a}$ because $\vec{g}\cdot\nu_2\vec{a}=2\pi$ if ν_2 is even. Thus S_1 can be evaluated by inserting a factor of $1=\exp[i\nu_1\vec{g}\cdot\vec{a}]\exp[-i\nu_1\vec{g}\cdot\vec{a}]$ giving

$$\begin{aligned} S_1 &= d\sum_{\nu_1=0}^{\infty} \exp\{i[(k'_{\perp}+k_{\perp})d-\vec{g}\cdot\vec{a}]\nu_1\} \times \sum_{\gamma=0}^{\infty} \exp\{i[(k_{\perp}+k)d-\vec{g}\cdot\vec{a}]\gamma\} \\ &= d(1-\exp\{i[(k'_{\perp}+k_{\perp})d-\vec{g}\cdot\vec{a}]\})^{-1} \times (1-\exp\{i[(k_{\perp}+k)d-\vec{g}\cdot\vec{a}]\})^{-1}\,. \end{aligned} \qquad \text{(A2)}$$

Equation (A2) is not directly useful for evaluating the limit in which the boson field is regarded as being characteristic of a uniform medium rather than a periodic solid. In this case we must replace S_1 with its precise definition. [We included the d factor from Ω = unit-cell volume = Ad in the coupling constants given by Eqs. (2.15), (2.17), and (2.18) in the definition of S_1.] This definition is obtained from (A1) to be

$$\begin{aligned} S_1 &= \sum_{\nu_1=0}^{\infty} \int_{d\nu_1}^{d(\nu_1+1)} \exp[i(k'_{\perp}-k)x]\,dx \times \sum_{\nu_2=\nu_1}^{\infty} \exp[i(k_{\perp}+k)d\nu_2 - i\vec{g}\cdot\vec{a}_2] \\ &= \left(\frac{\exp[i(k'_{\perp}-k)d]-1}{i(k'_{\perp}-k)}\right) \frac{1}{1-\exp\{i[(k'_{\perp}+k_{\perp})d-\vec{g}\cdot\vec{a}]\}} \times (1-\exp\{i[(k_{\perp}+k)d-\vec{g}\cdot\vec{a}]\})^{-1}\,. \end{aligned} \qquad \text{(A3)}$$

Note that we take the continuum limit of the ν_1 sum prior to performing the ν_2 sum. Otherwise the factor $-kx$ in the integral in (A3) would be replaced by $k_{\perp}x$. Such a replacement would require that the net phase of the "central-cell structure factor," given by the quantity in bold parentheses in Eq. (A3),

is determined by sums over cell-periodic functions. As such a requirement is evidently incorrect, our ordering of the operations of integration and summation is unique.

The structure factor in Eq. (A3) occurs in our model only for continuum loss-mode vertices. It has the effect of multiplying the $t_n(\vec{k}', \vec{k}, \vec{p})$ in Eqs. (2.13a), (2.14), (2.15), and (2.17) by the structure factor

$$F_\perp(\vec{k}', \vec{k}, \vec{p}) = \left(\frac{\exp[i(k_\perp - k'_\perp - p_\perp)d] - 1}{i(k_\perp - k'_\perp - p_\perp)d}\right) \quad . \quad \text{(A4)}$$

However, as at the loss vertices we already have noted that only forward scattering occurs, i.e., $(k'_\perp + p_\perp - k_\perp) \ll d^{-1}$, we see that $F_\perp \cong 1$ for the parameters of interest in our calculation. Consequently we have neglected such structure factors in Sec. II.

Finally, the continuum limit is obtained by neglecting the cell-periodic nature of the solid. For example, in this limit the ν_1 sum in Eq. (A3) is converted to an integral by taking $d \to 0$. This prescription gives $[k'_\perp + k_\perp]^{-1}$ in lieu of the product of the first two factors on the right-hand side of Eq. (A3). The only sensible definition of this limit seems to be via systematically setting $d \to 0$ in (A3) because of the indeterminacy of the upper limit on the ν_2 sum in any other prescription. Practically speaking, the "continuum" nature of the loss-mode fields has the consequence of justifying power-series expansions of exponentials in forward-scattering diagrams (e.g., $F_\perp \to 1$), but exerting negligible effect on back-scattering diagrams because in actual situations the $k_\perp(\vec{g}, E)$ are never small relative to d^{-1}. Stated alternatively, a complete $d \to 0$ continuum limit eliminates the ability of the lattice periodic potential to cause back-scattering "umklapp" electronic transitions. Therefore, the application of this limit to estimate back-scattering factors from the ν_i sums in Eq. (A3) has no meaning.

---

*Research supported in part by the Advanced Research Projects Agency under Contract No. HC 15-67-C-0221.

†Present address: Sandia Laboratories, Albuquerque, N. M. 87115.

[1]C. Davisson and L. H. Germer, Phys. Rev. 30, 705 (1927).

[2]J. C. Turnbull and H. E. Farnsworth, Phys. Rev. 54, 507 (1938).

[3]P. P. Reichertz and H. E. Farnsworth, Phys. Rev. 75, 1902 (1949).

[4]J. O. Porteus, in *The Structure and Chemistry of Solid Surfaces*, edited by G. A. Somorjai (Wiley, New York, 1969), p. 12-1.

[5]W. H. Weber and M. B. Webb, Phys. Rev. 177, 1103 (1969).

[6]M. P. Seah, Surface Sci. 17, 161 (1969).

[7]C. B. Duke, G. E. Laramore, and V. Metze, Solid State Commun. 8, 1189 (1970); C. B. Duke and G. E. Laramore, Program of the Thirtieth Annual Conference on Physical Electronics (unpublished), Paper C7; *Proceedings of the Fourth Low Energy Electron Diffraction Theory Seminar* (University of California, Irvine, 1970), p. 10.

[8]C. B. Duke, A. J. Howsmon, and G. E. Laramore, J. Vacuum Sci. Technol. 8, 10 (1971).

[9]M. Born, Rept. Progr. Phys. 9, 294 (1942).

[10]L. Van Hove, Phys. Rev. 95, 249 (1954).

[11]C. Kittel, *Quantum Theory of Solids* (Wiley, New York, 1963), Chaps. 19 and 20.

[12]R. F. Wallis and A. A. Maradudin, Phys. Rev. 148, 962 (1966).

[13]D. L. Huber, Phys. Rev. 153, 772 (1967).

[14]J. T. McKinney, E. R. Jones, and M. B. Webb, Phys. Rev. 160, 523 (1967).

[15]R. T. Barnes, M. G. Lagally, and M. B. Webb, Phys. Rev. 171, 627 (1968).

[16]M. G. Lagally and M. B. Webb, Phys. Rev. Letters 21, 1388 (1968); *The Structure and Chemistry of Solid Surfaces*, edited by G. A. Somorjai (Wiley, New York, 1969), p. 20-1.

[17]R. E. Wames and L. A. Vredevoe, Phys. Rev. Letters 20, 853 (1967).

[18]D. L. Mills, J. Phys. Chem. Solids 28, 2245 (1967).

[19]Y. H. Ohtsuki, J. Phys. Soc. Japan 24, 555 (1968).

[20]E. N. Economou, M. H. Cohen, and K. L. Ngai, in Proceedings of the Fourth LEED Theory Seminar, (unpublished) p. 112, Phys. Rev. Letters 24, 61 (1970).

[21]N. F. Mott and H. S. W. Massey, *The Theory of Atomic Collisions*, 3rd ed. (Clarendon, Oxford, England, 1965), Chap. 13.

[22]A. M. Afanas'ev and Yu Kagan, Acta. Cryst. A24, 163 (1967), and references therein.

[23]R. E. De Wames, W. F. Hall, and G. W. Lehman, Phys. Rev. 148, 181 (1966).

[24]D. L. Mills and V. Roundy, in *Proceedings of the Fourth Low Energy Electron Diffraction Theory Seminar* (University of California, Irvine, 1970).

[25]E. G. McRae and P. J. Jennings, in *The Structure and Chemistry of Solid Surfaces*, edited by G. A. Somorjai (Wiley, New York, 1969), p. 7-1.

[26]J. C. Slater, Phys. Rev. 51, 840 (1937).

[27]C. B. Duke and C. W. Tucker, Jr., Surface Sci. 15, 231 (1969).

[28]R. O. Jones and J. A. Strozier, Jr., Phys. Rev. Letters 22, 1186 (1969).

[29]C. B. Duke and C. W. Tucker, Jr., Phys. Rev. Letters 23, 1163 (1969).

[30]E. Bauer, Z. Physik 224, 19 (1969).

[31]J. I. Gersten, Phys. Rev. 188, 774 (1969).

[32]Y. H. Ohtsuki, J. Phys. Soc. Japan 29, 398 (1970).

[33]J. O. Porteus and W. N. Faith, Phys. Rev. B 2, 1532 (1970).

[34]C. B. Duke and G. E. Laramore, Phys. Rev. B 2, 4765 (1970).

[35]D. J. Scalapino, in *Superconductivity*, edited by R. D. Parks (Marcel Dekker, New York, 1969), Vol. I, pp. 449–558.

[36]T. M. Rice, Ann. Phys. (N. Y.) 31, 100 (1965).

[37]Similar conclusions have been reached in studies of the high-frequency "optical" properties of metals. See, e.g., L. W. Beefreman and H. Ehrenreich, Phys. Rev. B 2, 364 (1970), and references therein.

[38]C. B. Duke, J. R. Anderson, and C. W. Tucker, Jr.,

Surface Sci. 19, 117 (1970).

[39]J. B. Pendry, J. Phys. C 1, 1065 (1968).

[40]J. A. Strozier, Jr. and R. O. Jones, Phys. Rev. Letters 25, 516 (1970).

[41]V. Hoffstein and D. S. Boudreaux, Phys. Rev. Letters 25, 512 (1970).

[42]C. B. Duke, J. Vacuum Sci. Technol. 6, 152 (1969).

[43]N. D. Lang and W. Kohn, Phys. Rev. B 1, 4555 (1970).

[44]C. W. Tucker, Jr. and C. B. Duke, Surface Sci. 24, 31 (1971).

[45]L. Hedin and S. Lundquist, Solid State Phys. 23, 1 (1969).

[46]J. B. Pendry, J. Phys. C 2, 1215 (1969).

[47]M. Ichikawa and Y. H. Ohtsuki, J. Phys. Soc. Japan 27, 953 (1969).

[48]R. M. Goodman, H. M. Farrell, and G. A. Somorjai, J. Chem. Phys. 49, 692 (1968).

[49]R. M. Stern and A. Gervais, Surface Sci. 17, 273 (1969).

[50]H. Tokutaka and J. A. D. Matthew, Surface Sci. 19, 427 (1970).

[51]A. A. Abrikosov, L. P. Gorkov, and I. E. Dzyaloshinski, *Methods of Quantum Field Theory in Statistical Physics*, translated by R. A. Silverman (Prentice-Hall, Englewood Cliffs, N. J., 1963), pp. 135–139, 176–188.

[52]C. B. Duke, M. J. Rice, and F. Steinrisser, Phys. Rev. 181, 733 (1969).

[53]P. Nozières, *Theory of Interacting Fermion Systems*, translated by D. Hone (Benjamin, New York, 1964), pp. 221–237.

[54]G. E. Laramore and C. B. Duke, Phys. Rev. B 3, 3198 (1971).

[55]G. E. Laramore and C. B. Duke, Phys. Rev. B 2, 4783 (1970).

[56]S. S. Schweber, *An Introduction to Relativistic Quantum Field Theory* (Row, Peterson, and Company, Evanston, Ill., 1961), Chaps. 11, 13, 14.

[57]In Ref. 7, C. B. Duke *et al.* do not permit $R_{1m}=R_{1n}$. Therefore their expressions for A [Eq. (3a) in Ref. 7] contain an extra factor of R in the numerator relative to those given herein. The question at issue is whether or not we permit loss and elastic scattering in the same lattice cell. As we view the loss as due to a distributed excitation of the valence electrons, it seems most reasonable to permit both process to coexist in a given cell and hence our change in boundary condition. Presumably the correct boundary condition ultimately will be determined by comparison of the model predictions with experimental data.

[58]Our heuristic prescription for performing the lattice sums neglects the coupling of the electron to the electrostatic field of the surface plasmons outside of the solid. In the absence of damping inside the crystal, this restriction is easily removed. In the presence of damping as described in the text, this restriction causes errors in the magnitude of the intensity profiles of order unity, but no qualitative changes in the line shape. For example, although the cross section determined by Eqs. (4.16) does not vanish as $|\vec{k}'_{\parallel}-\vec{k}_{\parallel}-\vec{g}|\to 0$, it does become small. The corresponding result in the second-order perturbation-theory expression, Eq. (4.6), is discussed following Eqs. (4.7). However, in the case of the fourth-order cross sections, the restrictions on the sums over $\vec{R}_n$ described in the Appendix prevent the vanishing of $(d^2\tau/dE\,d\Omega)^{(4)}$ when $|\vec{k}'_{\parallel}-\vec{k}_{\parallel}-\vec{g}|\to 0$ even for plane-wave electrons. We currently are reexamining the role of these restrictions within the context of deriving an appropriate microscopic theory of electron damping due to its simultaneous interaction with both surface plasmons and (dissipative) bulk particle-hole excitations in the solid.